THE JOURNAL OF PHYSICAL CHEMISTRY B

Article

pubs.acs.org/JPCB

Role of Carboxylate Side Chains in the Cation Hofmeister Series

Jaibir Kherb, Sarah C. Flores, and Paul S. Cremer*

Department of Chemistry, Texas A & M University, College Station, Texas 77843, United States

Supporting Information

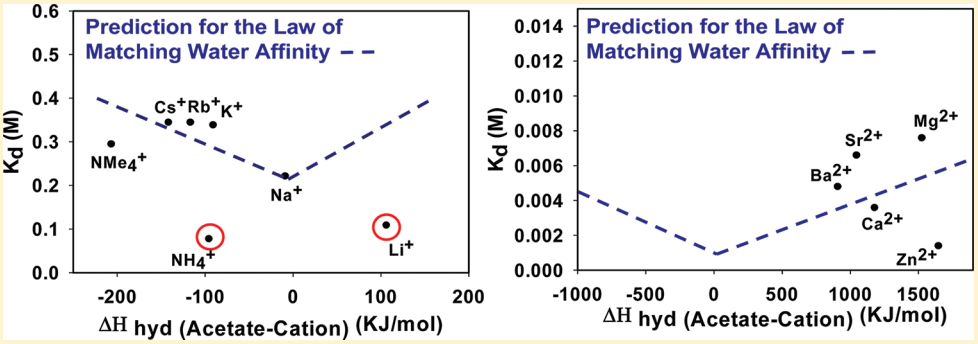

ABSTRACT: Thermodynamic and surface-specific spectroscopic investigations were carried with an elastin-like polypeptide (ELP) containing 16 aspartic acid residues. The goal was to explore the role of the carboxylate moieties in hydrophobic collapse and related Hofmeister effects. Experiments were conducted with a series of monovalent and divalent metal chloride salts. Both phase transition temperature and spectroscopic data demonstrated that the divalent cations showed relatively strong association to the carboxylate sites on the biopolymer with K_d values in the range of 1 to 10 mM. The ordering of the divalent series was: $Zn^{2+} > Ca^{2+} > Ba^{2+} > Sr^{2+} > Mg^{2+}$. Monovalent cations displayed weaker binding which ranged from 78 mM for NH_4^+ to 345 mM for Cs^+. The order for this series was: $NH_4^+ > Li^+ > Na^+ > NMe_4^+ > K^+ > Rb^+ \geq Cs^+$. These results are in general agreement with the notion that strongly hydrated cations bind more tightly to carboxylate groups than do weakly hydrated cations. Moreover, the data for the monovalent series was partially consistent with the law of matching water affinity, although Li^+ and NH_4^+ did not follow the model. The series for the divalent cations did not appear to obey the law of matching water affinity at all.

INTRODUCTION

The effects of salts on protein solubility and stability have been known for more than a century and were first reported by Franz Hofmeister.[1,2] These specific ion effects were later shown to be important for numerous biological and chemical phenomena ranging from protein−protein interactions and enzyme stability to DNA−protein interactions and ion-channel function.[3−9] Ionic effects also modulate tubulin polymerization[10] and vesicle stabilization.[11,12] A variety of inorganic ions has been tested for their ability to precipitate various proteins from solution. The overall order of a particular anion's and cation's effectiveness as a protein precipitant is generally as follows:

$$CO_3^{2-} > SO_4^{2-} > S_2O_3^{2-} > H_2PO_4^- > F^- > Cl^- > Br^- > NO_3^- > I^- > ClO_4^- > SCN^-$$

$$N(CH_3)_4^+ > NH_4^+ > Cs^+ > Rb^+ > K^+ > Na^+ > Li^+ > Ca^{2+} > Mg^{2+}$$

Anions to the left of chloride are well hydrated and help salt proteins out of solution. Anions to the right of chloride generally salt proteins into solution and are more weakly hydrated. The salting-out anions have a higher charge-to-volume ratio and generally have fairly weak polarizabilities. Salting-in anions, on the other hand, possess less charge per unit volume and are typically more strongly polarizable. Curiously, this trend reverses for cations. In that case, the largest and least charged cations are most effective at salting proteins out of solution, while divalent metal cations can lead to increased protein solubility.

There has been debate over the years as to whether the salting-in and salting-out effects of ions are related to bulk water properties. More recently, consensus has begun to emerge around the idea that salting-in and salting-out effects are more closely related to an ion's binding to or depletion from the protein/water interface.[13−16] For uncharged systems, such interactions should be with the amide backbone of a protein rather than hydrophobic side chains.[17−19] The influence of cations on the thermodynamic properties of uncharged systems is typically found to be weaker than for anions. As a result, the specific effects of cations, even though very important, have been harder to observe. Some recent molecular dynamics simulations have suggested that cations interact with the carbonyl oxygen on the amide backbones of proteins.[20]

Received: December 19, 2011
Revised: May 28, 2012
Published: June 14, 2012

   dx.doi.org/10.1021/jp212243c | J. Phys. Chem. B 2012, 116, 7389−7397

For systems containing sites of negative charge, the influence of cations can be much more pronounced. In fact, ion-pairing between mobile cations in solution and fixed titratable acetate groups on biomacromolecules is thought to affect protein−protein associations, protein folding/stability as well as macromolecular aggregation and precipitation.[10,20−22] The exact nature of these interactions should be ion specific as well as depend on the nature and charge distribution along the protein. Some clues about the mechanisms of these interactions can be gleaned from the analogous problem of the interactions of ions with synthetic polyelectrolytes.[23−28] Nevertheless, the ion specific nature of the interactions between sites of negative charge on proteins and cations still remains poorly understood.

The nature of cation interactions with sites of negative charge on proteins is inherently interfacial. Indeed, such interactions take place at the macromolecule/water interface. As such, surface specific techniques, such as vibrational sum frequency spectroscopy (VSFS), can potentially provide very useful vibrational information about these interactions.[29−32] Herein, we used VSFS experiments along with complementary thermodynamic data to help elucidate the nature of cation-acetate interactions. To do this, we employed specifically designed elastin-like polypeptides. The ELPs consisted of repeat units of the pentapeptide, Val-Pro-Gly-Xaa-Gly, where Xaa could be any amino acid residue except proline. These polypeptides are highly soluble in water at room temperature. When heated above their lower critical solution temperature (LCST),[15,33,34] the ELPs undergo hydrophobic collapse and aggregation. The phase transition temperature can be easily identified macroscopically by noting where an initially clear aqueous solution turns cloudy.

The relative hydrophobicity/hydrophilicity of ELPs can be tuned by inserting specific amino acid residues at the guest residue location in the constituent pentapeptide units. In this particular study, we employed a polypeptide containing aspartic acid residues at one-quarter of the guest residue sites. The other three-quarters of the sites contained hydrophobic valine and phenylalanine residues. The total chain length of the ELP was 320 amino acids long or 64 pentapeptide repeats. It is designated ELP DV_2F-64, which refers to the fact that aspartic acid, valine and phenylalanine residues are present in the guest residue position in a 1:2:1 ratio. Since there are 64 pentapeptides, the macromolecule possesses 16 aspartic acid residues, which imparts a significant negative charge at neutral and basic pH values. LCST and VSFS measurements indicated that the phase transition temperature of the biopolymer could be correlated with the binding affinities of the cations. The data followed a direct Hofmeister series. In the case of monovalent cations, a correlation could mostly be made between a cation's enthalpy of hydration and that of acetate on the one hand and the apparent dissociation constant between the cation and acetate on the other. Namely, the closer the known solvation enthalpy of the cation was to that of an acetate moiety, the tighter the apparent binding constant would be. The two exceptions to this were Li^+ and NH_4^+, which both showed tighter binding than the model would predict. This is in partial agreement with the proposed law of matching water affinity (LMWA).[35−37] However, no such correlation could be found for the divalent cations.

EXPERIMENTAL SECTION

LiCl, NaCl, KCl, RbCl, CsCl, NH_4Cl, NMe_4Cl, $MgCl_2$, $CaCl_2$, $SrCl_2$, $BaCl_2$, $ZnCl_2$, tris(hydroxymethyl)-aminomethane, and tris(hydroxymethyl) aminomethane hydrochloride buffers were purchased from Sigma-Aldrich. The salt purities were: 99.9% for LiCl, 99.999% for NaCl, 99.999% for KCl, 99.8% for RbCl, 99.999% for CsCl, 99.995% for NH_4Cl, 99.9% for $NMeCl_4$, 99.9% for $MgCl_2$, 99.99% for $CaCl_2$, $SrCl_2$ 99.995% for $SrCl_2$, 99.999% for $BaCl_2$, and 99.999% for $ZnCl_2$. All salt solutions and buffers were prepared by dissolving the dry salts in freshly purified deionized water obtained from a NANOpure Ultrapure Water System (Barnstead, Dubuque, IA) having a minimum resistivity of 18.1 MΩ.cm. For VSFS experiments in heavy water, salt solutions were prepared in 99.9% isotopically pure D_2O, which was obtained from Cambridge Isotope Laboratories, Inc. (Andover, MA).

It should be noted that the zinc salts can form zinc hydroxide in alkaline solutions.[38,39] Under the conditions employed in the current experiments, the pH of the ELP solutions was set to 9.76 in 10 mM Tris (hydroxymethyl)-aminomethane buffer. The addition of most salts did not alter this value. However, the pH dropped to 9.26 when 1 M $ZnCl_2$ was added to the solution. It should be noted that this change had almost no effect on the LCST of the ELP (Supporting Information, Figure S1). Also, the pK_a for the NH_4^+ ion is close to pH 9.25; hence, at pH 9.76, only 24 mol % of this species was in the form of NH_4^+, while the rest converted to NH_3.

ELP Preparation. pET plasmids having an inserted gene sequence for ELP DV_2F-64 were obtained from the Chilkoti laboratory at Duke University. These were constructed using recursive directional ligation.[40] The plasmids were transformed into BLR (DE3) competent *Escherichia coli* cells (Novagen, MERCK Chemicals). The cells were expressed for 24 h at 37 °C in TB Dry cell culture growth medium (MO Bio Laboratories, Inc.). Expression was done in ampicillin containing medium so as to prevent the growth of undesired bacteria. Cells were then lysed via sonication and the cell debris was removed using centrifugation. Treatment of the resulting supernatant with poly(ethyleneimine) led to the removal of unwanted nucleic acids. The ELP's inverse phase transition temperature and sensitivity toward inorganic salts was exploited for the isolation and purification of the biopolymer. Specifically, lysate solutions were subjected to a series of inverse transition cycles (ITC). To do this, 1 M NaCl was added to the solution followed by incubation at 50 °C for 1 h. This caused the ELP to precipitate out of solution. This white precipitate was collected as a pellet via centrifugation and the pellet was then redissolved in cold sodium phosphate buffer (10 mM, pH 7). Generally, 2−3 rounds of ITC were sufficient to remove all unwanted impurities. Sodium dodecyl sulfate-polyacrylamide gel electrophoresis (SDS-PAGE) was performed to confirm the purity and molecular weight of the final product. The concentration of ELP molecules in aqueous solution was determined by UV absorbance measurements at 280 nm (ε = 5690 $M^{-1}cm^{-1}$).[40] Dialysis of the final purified polypeptide solution was done against purified water to remove any residual salts. Finally, the polypeptide samples were lyophilized and stored at −80 °C until their use in thermodynamic and spectroscopic measurements.

LCST Measurements. Stock solutions (1 M) of all of the monovalent and divalent chloride salts were prepared in 10 mM Tris buffer at pH 9.76. Salt solutions of the desired concentration were obtained by diluting the stock solutions with pure buffer. For all thermodynamic measurements, lyophilized solid samples of ELP DV_2F-64 were dissolved in aqueous salt solutions to obtain a final peptide concentration of

10 mg/mL. Prior to making LCST measurements, all peptide solutions were kept in an ice bath for ~30 min to ensure complete solubilization. The phase transition temperature measurements were made with an automated melting point apparatus (Optimelt MPA 100, Stanford Research Systems). In a typical LCST measurement, three capillary tubes filled with identical ELP solutions were placed in the heating chamber of the melting point device. The samples were then subjected to a gradual temperature ramp and the light scattering intensity of the samples was recorded as a function of temperature. A ramp rate of 0.5 °C/min was used for all measurements. The built-in camera on the instrument captured real-time images of the samples and then used digital image processing software to determine the onset of the LCST. All LCST values reported in this study consisted of an average of six measurements. The data obtained was highly reproducible and used just ~10 μL of ELP sample per capillary tube.

VSFS Measurements. In VSFS experiments, a visible beam and an IR beam were temporally and spatially overlapped at the sample surface to generate a sum-frequency response.[29−32] Enhancement in the sum frequency signal was observed when the incoming IR beam was on resonance with vibrationally active moieties at the surface. VSFS spectra were taken with a standard VSFS setup as described in detail elsewhere.[31,32] Briefly, a passive-active mode locked Nd:YAG laser (PY61c, Continuum, Santa Clara, CA) equipped with a negative feedback loop in the oscillator cavity was used to generate a 1064 nm laser beam of 50 mJ/pulse with a 17 ps pulse duration. The laser operated at 20 Hz. The 1064 nm beam was then sent through an optical parametric generation/amplification (OPG/OPA) stage (LaserVision, Bellevue, WA) which resulted in the production of a frequency-doubled visible beam (532 nm) and a tunable mid-infrared beam. The frequency of the IR beam could be tuned from 2000 to 4000 cm^{-1}. The visible and infrared beams were then spatially and temporally aligned at an air/water interface in a Langmuir trough and the resulting VSFS signal was collected using a photomultiplier tube (Hamamatsu, Japan). In this particular study, the IR beam was continuously tuned between 2750 cm^{-1} to 3800 cm^{-1} with a power of ~0.6 mJ/pulse at the sample stage near 3000 cm^{-1}. The power of incoming 532 nm beam was 1 mJ/pulse.

To take a VSFS measurement, 35 mL of a salt solution were placed in the Langmuir trough (Model 601M, Nima, U.K.). Next, a 40 μL droplet of a 10 mg/mL stock solution of ELP DV_2F-64 was added to the top of the salt solution in the trough. This concentration of polypeptide was sufficient to rapidly form a highly reproducible saturated Gibbs monolayer at the air−water interface. Control experiments demonstrated that increasing the concentration of the added polypeptide solution did not affect the VSFS spectrum. An equilibration time of 10 min was given for the monolayer to be stabilized before starting a VSFS experiment. Longer waiting times were found to have negligible impact on the obtained spectral profiles and intensities. All the spectra were collected with the ssp (s-sum frequency beam, s-visible beam, p-infrared beam) polarization combination. The VSFS spectra taken in this study were all collected over a time period of approximately 40 min.

In a VSFS experiment, the intensity of the sum frequency generation signal, I_{SFG}, is proportional to the intensities of the input visible, I_{vis}, and infrared, I_{IR}, laser beams:

$$I_{SFG} \propto |\chi_{eff}^{(2)}|^2 \times I_{vis} \times I_{IR} \quad (1)$$

Where $\chi_{eff}^{(2)}$ is the effective second order nonlinear susceptibility which can be further expressed as:

$$\chi_{eff}^{(2)} = \chi_{NR}^{(2)} + \chi_{R}^{(2)} = \chi_{NR}^{(2)} + \sum_q \frac{A_q}{\omega_{IR} - \omega_q + i\Gamma_q} \quad (2)$$

Here, $\chi_{NR}^{(2)}$ is the frequency-independent nonresonant term and $\chi_{R}^{(2)}$ is frequency- dependent resonant term. Furthermore, $\chi_{R}^{(2)}$ of the qth resonant mode can be written as a function of the oscillator strength, A_q, the resonant frequency, ω_q, the peak width, Γ_q, and the frequency of the input infrared laser, ω_{IR}.

RESULTS

LCST Data of ELP DV_2F-64 with Chloride Salts. Phase transition temperature measurements of 10 mg/mL aqueous solutions of ELP DV_2F-64 at pH 9.76 were measured as a function of salt type and concentration for 12 different chloride salts. Under these solution conditions, the acidic polypeptide residues were almost completely deprotonated (Supporting Information, Figure S1). This pH and peptide concentration were chosen to allow thermodynamic measurements to be carried out over a wide range of temperatures and salt concentrations. Figure 1 shows the effect of divalent chloride

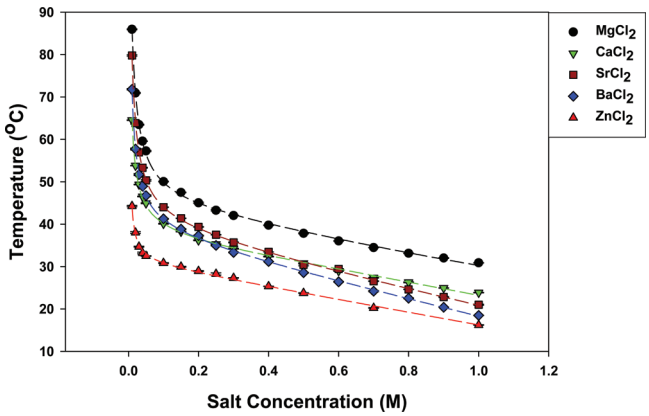

Figure 1. LCST response of ELP DV_2F-64 as a function of the concentration and identity of divalent metal chlorides. All experiments were performed with 10 mg/mL ELP in 10 mM Tris buffer at pH 9.76. Each data point represents an average of six measurements and the dashed lines are the best fits to the data points.

salts on the LCST value of the ELP for divalent metal cations in a range from 0 to 1 M salt. The addition of these salts to the polypeptide solution imparted an exponential decrease in the phase transition temperature below 100 mM salt. A shallower more linear decrease was found as the salt concentration was further increased. The order of decrease at the lowest salt concentrations employed was: Zn^{2+} > Ca^{2+} > Ba^{2+} > Sr^{2+} > Mg^{2+}. In other words, Zn^{2+} depressed the LCST the most in this regime, while Mg^{2+} lowered this value the least. The order rearranged at higher salt concentrations to Zn^{2+} > Ba^{2+} > Sr^{2+} > Ca^{2+} > Mg^{2+}. In other words, the relative position of Ca^{2+} changed substantially.

Figure 2 shows the analogous thermodynamic data for ELP DV_2F-64 in the presence of increasing concentrations of monovalent chloride salts. The overall trends are similar to the divalent cations. However, the initial exponential decrease in the LCST took place up to 500 mM salt. The ordering of the initial decrease was: NH_4^+ > Li^+ > Na^+ > K^+ > Rb^+ ≥ Cs^+ >

dx.doi.org/10.1021/jp212243c | J. Phys. Chem. B 2012, 116, 7389−7397

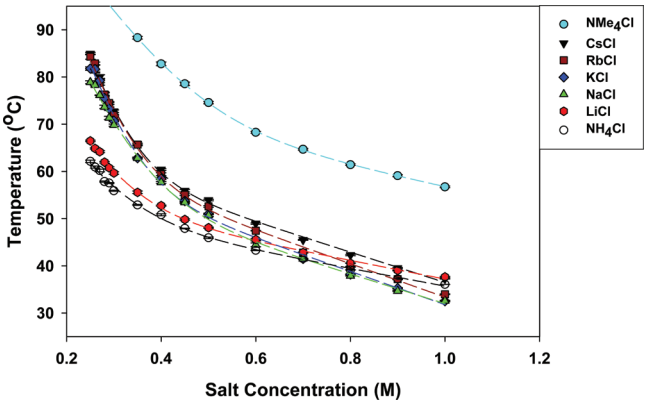

Figure 2. LCST response of ELP DV_2F-64 as a function of the concentration and identity of monovalent chloride salts. All experiments were performed with 10 mg/mL ELP in 10 mM Tris buffer at pH 9.76. Each data point represents an average of six measurements and the dashed lines are the best fits to the data points.

NMe_4^+. Again, there was considerable rearrangement in the ordering at higher salt concentrations, which became: $Na^+ \sim K^+ > Rb^+ > NH_4^+ > Cs^+ > Li^+ > NMe_4^+$.

Fitting of the Thermodynamic Data. At pH 9.76, the aspartic acid residues on the peptide surface exist in their deprotonated form. This imparts a high negative charge on the ELP. As a result, the initial LCST of the ELP is quite high because of electrolytic repulsion between the negatively charged groups. In fact, the boiling point of the aqueous solution in the absence of salt was reached before the LCST could be observed. Addition of salts should result in ion pairing between cations in solution and the carboxylate moieties.[20,21] This neutralizes the negative charge on the biopolymer, which allows the inverse phase transition to take place at lower temperatures. Such ion pairing between the acetate moieties and free cations in addition to charge screening should be correlated to the exponential decrease in the ELP collapse temperature at low salt concentrations.[41] Once this relatively strong ion pairing interaction is saturated, the significantly weaker interactions of the ions with the peptide backbone and hydrophobic residues become the dominant factor in modulating the LCST. These latter interactions, which generally involve the exclusion of ions from the polymer/aqueous interface, lead to salting-out of the ELP. This is strongly correlated with increasing surface tension as the ionic strength is increased.[14,15] It has recently been proposed that the molecular level origin of this salting-out effect involves dispersion forces of the ions.[42,43]

The two types of interactions governing the LCST can be modeled using eq 3, which consists of a constant, a modified Langmuir binding isotherm and a linear term:[41]

$$T = T_0 + c[M] + \frac{B_{max}[M]e^{-b[M]^2}}{K_d + [M]e^{-b[M]^2}} \quad (3)$$

where T_0 is the phase transition temperature of the ELP in the absence of added salt and [M] is the molar salt concentration. The constant, B_{max}, has units of temperature and denotes the maximum decrease in the LCST when all of the acetate moieties on the ELP are paired with cations. The constant, b, has units of inverse molarity and is related to the strength of the electrostatic interactions between the negatively charged polypeptide and the cations. The constant, K_d, represents the apparent dissociation constant for the specific interactions of the cations to the putative acetate binding sites. The lower the value of K_d, the stronger the binding affinity should be. The constant, c, has units of temperature/molarity and represents the linear change in the interfacial tension of the polypeptide/water interface as salt is added to the solution. It should be noted that the square of the molar concentration in the exponential term yielded an excellent fit to the data, while choosing $[M]^{1/2}$, [M], or $[M]^3$ in the exponential term did not. This fit should be considered phenomenological. The dashed lines in Figure 1 and Figure 2 are the fits of the experimental data to eq 3. As can be seen, the fits are quite good. From the fitting of all the monovalent and divalent salts, the extrapolated value of T_0 is ~140 °C. The abstracted values of K_d, B_{max}, b, and c obtained from fitting are summarized in Table 1.

Table 1. Fitted Values of the Parameters Obtained from Employing Eq 3 to the LCST Data of ELP DV_2F-64

cation	B_{max} (°C)	K_d (M)	b (M^{-1})	c (°C/mol)
Mg^{2+}	−94.7	0.0076	−5.73	−14.9
Ca^{2+}	−102.0	0.0036	−4.68	−14.4
Sr^{2+}	−99.9	0.0066	−2.66	−19.2
Ba^{2+}	−101.0	0.0048	−5.12	−20.6
Zn^{2+}	−109.0	0.0014	−0.24	−14.8
Li^+	−82.8	0.109	−12.1	−19.9
Na^+	−76.5	0.222	−11.0	−31.4
K^+	−72.9	0.339	−15.9	−35.2
Rb^+	−71.1	0.345	−16.2	−35.4
Cs^+	−71.2	0.345	−16.8	−32.1
NH_4^+	−85.4	0.078	−10.4	−18.8
NMe_4^+	−61.2	0.295	−6.20	−21.9

As can be seen from the table, the apparent dissociation constants, K_d, of the cations to the ELP surface are somewhat below 10 mM for the divalent cations and below 1 M for the monovalent cations. There is roughly a 2 orders of magnitude difference in affinity between these groups. At the extreme, the difference in K_d between Zn^{2+} and Rb^+ is about 250 fold. By contrast with the dissociation constant data, the ranges for the other constants are much narrower. Specifically, the B_{max} values for the divalent cations are clustered around 100 °C, whereas the monovalent numbers are closer to 80 °C with the exception of NMe_4^+, which is modestly lower. Also, the values of the b constants cluster around −10 to −15 for the monovalent cations, but are near −5 for Mg^{2+}, Ca^{2+}, Sr^{2+}, and Ba^{2+}. This difference should reflect the greater screening afforded by the divalent metal ions. However, Zn^{2+} appears to be an exception as it exhibits a smaller b value. This may reflect differences in the mechanism of the collapse process with Zn^{2+}, a tendency to bind the carboxylate groups in a multivalent fashion, or even the slight increase in acidity as $ZnCl_2$ is added to solution. Finally, the linear portion of the salting out effect should be dominated by the influence of chloride anions on the surface tension rather than by the monovalent or divalent cations.[3,4,44,45] Indeed, the surface tension increments of the various chloride salts of the cations fall within a narrow range as the cation is varied (Table 2). The difference in c values even between Rb^+ and Mg^{2+} is only slightly greater than a factor of 2 (Table 1). The relatively large variation in K_d values with only smaller differences in the other variables is in agreement with the notion that specific cation effects are substantial for ion

dx.doi.org/10.1021/jp212243c | J. Phys. Chem. B 2012, 116, 7389−7397

Table 2. Literature Values of Enthalpies of Hydration and Surface Tension Increments of Cations[44,46]

ion	ΔH hydr (KJ/mol)	$\Delta\sigma^a$ (mN L/m mol)
Li^+	−531	1.63
Na^+	−416	1.64
K^+	−334	1.4
Rb^+	−308	1.56
Cs^+	−283	1.56
NH_4^+	−329	1.39
NMe_4^+	−218	0.6
Mg^{2+}	−1949	3.04
Ca^{2+}	−1602	3.2
Sr^{2+}	−1470	3.25
Ba^{2+}	−1332	2.97
Zn^{2+}	−2070	2.94

[a]All surface tension increment values are for the corresponding 1 M metal chloride salt solution. The ionic strength difference between monovalent and divalent metal chloride should be taken into account when comparing the values. Moreover, the chloride concentration is double for the divalent metal salts.

pairing, but only modest for other factors affecting hydrophobic collapse.

As a control experiment, the LCST values of the ELPs were measured at pH 2.5 in the presence of the monovalent and divalent metal chloride salts (Supporting Information, Figure S2). The aspartic acid residues were mostly protonated under these conditions. In this case, only a shallow linear decrease in the LCST values was observed under all conditions as salt was added to solution. The differences among the cations were no more than 4 °C at 300 mM chloride salt for either the monovalent or divalent cations. Such experiments directly highlight the role that charged carboxylate groups play in obtaining the exponential portion of the phase transition curves as a function of salt concentration.

VSFS Spectral Features of ELP DV_2F-64. To obtain molecular level information on cation partitioning to the ELP/water interface, surface specific spectroscopic measurements were performed. VSFS measurements of a Gibbs monolayer of ELP DV_2F-64 were recorded at various salt concentrations and pH conditions. In a first set of experiments, VSFS spectra of an ELP DV_2F-64 monolayer were taken at a series of different pH values (Figure 3). Each spectrum had the same spectroscopic features in the CH stretch region (~2800−3100 cm^{-1}). The major peak near 2875 cm^{-1} arises from the symmetric stretch of the methyl groups on the valine residues. A very weak shoulder near 2840 cm^{-1} can also be seen, which is assigned to a CH_2 symmetric stretch. Another major peak was clearly visible at approximately 2950 cm^{-1}, which is generally attributed to a Fermi resonance of the methyl symmetric stretch as well as the slightly higher frequency methyl asymmetric stretch.[32] The weak band near 3050 cm^{-1} can be attributed to the aromatic CH stretch of the phenylalanine residues present on the ELP. The overall intensity from the CH region indicates a high degree of ordering of the polypeptide at the air/water interface. This is expected, as hydrophobic valine and phenylalanine side chains should be oriented into the air and away from the aqueous solution. There are some apparent differences in peak heights as a function of pH, but these are caused by constructive interference between the CH and OH stretch regions as can be demonstrated by control experiments in D_2O (Supporting Information, Figure S3).

The OH stretch region contains two distinct, broad spectral features. The first is centered around 3200 cm^{-1} and can be assigned to the OH stretch of interfacial water molecules in a mostly tetrahedral conformation.[30,32] The second prominent OH stretch peak, centered close to 3450 cm^{-1}, is typically assigned to water molecules that lack a full complement of hydrogen bonds. The oscillator strength in the OH region is highly sensitive to the pH of the bulk solution. This is expected as more aspartic acid residues become deprotonated as the pH is increased. Deprotonation imparts a strong negatively charged potential at the peptide/water interface, which should align the adjacent water layer. At sufficiently high pH, nearly all the acidic residues become deprotonated. This is nearly true by pH 7.29, but is certainly true by pH 9.76. These numbers are in excellent agreement with LCST data for ELP DV_2F-64, which shows a continuous rise in the inverse phase transition temperature starting around pH 2 and leveling off near pH 8 (Supporting Information; Figure S1).

Specific Binding of Cations to the Negatively Charged ELP Surface. To investigate the partitioning of divalent metal ions to the negatively charged peptide interface, VSFS spectra of ELP DV_2F-64 were taken at pH 9.76 in the presence of 16.66 mM of various divalent metal chloride salts (Figure 4). When

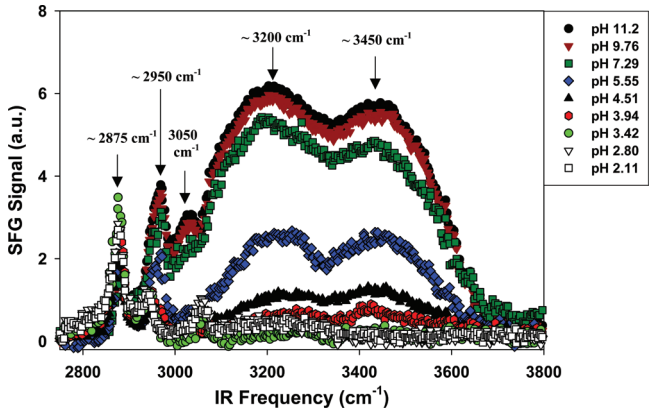

Figure 3. VSFS spectra of ELP DV_2F-64 as a function of pH. All experiments were performed with 1 mM Tris buffer. The pH was modulated by adding HCl.

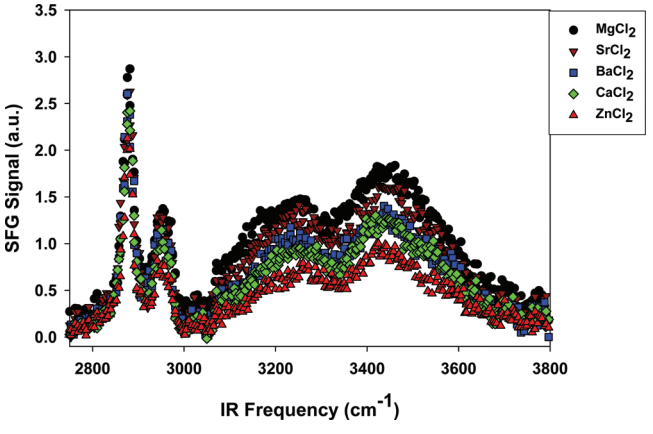

Figure 4. VSFS spectra of ELP DV_2F-64 in the presence of divalent metal chloride salts. All experiments were performed with a 16.66 mM concentration of chloride salt solutions in 1 mM Tris buffer at pH 9.76. Each spectrum represents an average of three scans.

dx.doi.org/10.1021/jp212243c | J. Phys. Chem. B 2012, 116, 7389−7397

the divalent metal ions bind to the negatively charged aspartate moieties, the interfacial charge is neutralized, leading to lower signal intensity in the OH stretch region. The relatively low salt concentration was chosen to correspond to the steep exponential decay portion of the LCST data in Figure 1. As can be seen from the data in Figure 4, the ion that led to the greatest attenuation in water signal intensity was Zn^{2+}, while Mg^{2+} had the smallest effect. The order of the ions was: Zn^{2+} > Ca^{2+} > Ba^{2+} > Sr^{2+} > Mg^{2+}. This is the identical order to that found at low salt concentrations in the thermodynamic data in Figure 1 and also matches the order of the apparent K_d values for the putative acetate-divalent cation binding data provided in Table 1.

Figure 5 shows the corresponding specific interactions observed with monovalent chloride ions at the same pH as in Figure 4, but with 50 mM salt. These conditions correspond to the exponential portion of the LCST data in Figure 2. The overall binding order was found to be: NH_4^+ > Li^+ ≥ Na^+ ≥ K^+ > Rb^+ ≥ Cs^+ > NMe_4^+. Again, this is identical to the low concentration ordering found in LCST data in Figure 2.

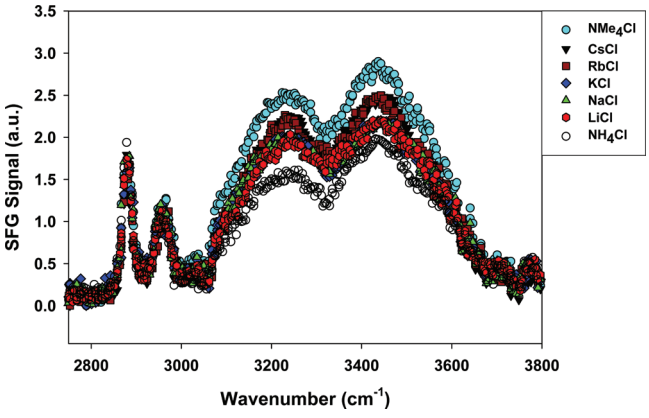

Figure 5. VSFS spectra of ELP DV_2F-64 in the presence of monovalent metal chloride salts. All experiments were performed with a 50 mM concentration of salt solutions in a 1 mM Tris buffer at pH 9.76. Each spectrum represents an average of three scans.

It should be noted that the VSFS spectra in both Figures 4 and 5 showed some very small apparent signal intensity changes even in the CH stretching region (2800−3100 cm^{-1}). These changes are the result of constructive interference with the OH stretch region and the actual CH stretch intensities remained unchaged. As with pH changes, this can be demonstrated by running control experiments in D_2O (Supporting Information, Figures S4 and S5). Such control experiments demonstrate that the surface concentration and orientation of the peptide remained essentially unchanged regardless of the particular salt that was employed. As such, the intensity changes in the spectra are a result of changes in the oscillator strength in the OH stretch region.[31]

VSFS Spectra of Protonated ELP DV_2F in the Presence of Salt. The presence of a significant number of negatively charged residues should be the overriding factor causing cation specificity in both the above VSFS and LCST data at low salt concentration. To test this hypothesis, the VSFS measurements were repeated at pH 2.7 under otherwise identical conditions to those shown above. Figure 6 shows the VSFS response for the divalent chloride salts, while the monovalent chloride salt data are in Figure 7. As can be clearly seen, all the spectra are essentially identical within experimental error. This means that ELPs with protonated aspartate residues lead to essentially no cation specific differences in the salt concentration range employed.

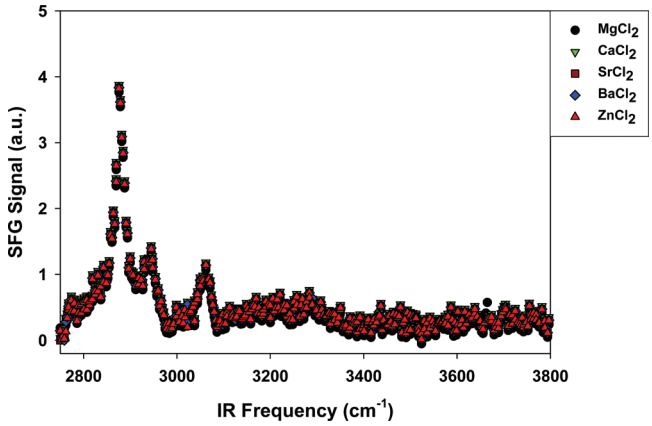

Figure 6. VSFS spectra of ELP DV_2F-64 at pH 2.7 in the presence of various divalent chloride salts. All experiments were performed with 16.66 mM salt in 1 mM Tris buffer.

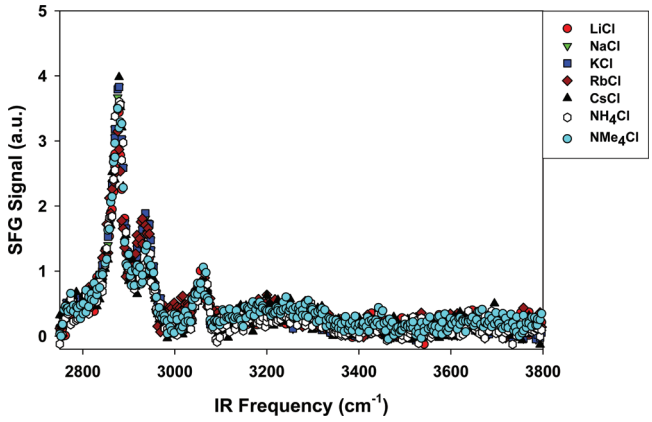

Figure 7. VSFS spectra of ELP DV_2F-64 at pH 2.7 in the presence of various monovalent chloride salts. All experiments were performed with 50 mM salt in 1 mM Tris buffer.

DISCUSSION

The thermodynamic data trends shown in Figure 1 and 2 are in agreement with the qualitative interfacial partitioning tendencies of the monovalent and divalent metal ions found by using VSFS. These data demonstrate that the apparent dissociation constants for the divalent cations with the aspartate acid residues on the ELPs range from ∼1 mM to ∼8 mM (Table 1). On the other hand, the strongest binding monovalent metal ion is Li^+ with an apparent dissociation constant of ∼109 mM. As such, the smallest difference in affinity between a monovalent and divalent metal cation is a factor of 14 between Mg^{2+} and Li^+. As noted above, Zn^{2+} has a dissociation constant which is ∼250 times tighter than Rb^+. The notion that divalent cations bind to acetate between one and three orders of magnitude more tightly than monovalent cations is consistent with qualitative experiments describing the interactions of cations with negatively charged synthetic polyelectrolytes, peptides, nucleic acids and fatty acid headgroups.[39,47−53] Such relative differences in interaction strengths may be a key reason for the presence of divalent ions in catalytic sites of numerous proteins

dx.doi.org/10.1021/jp212243c | J. Phys. Chem. B 2012, 116, 7389−7397

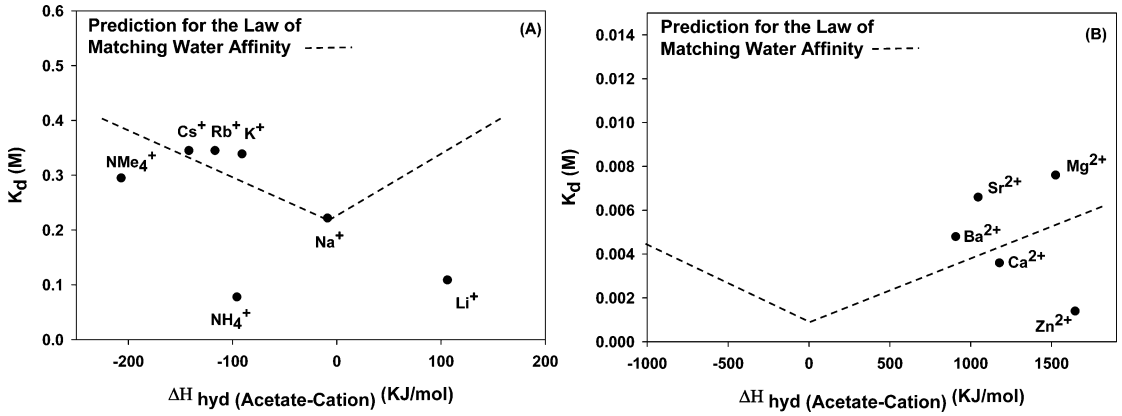

Figure 8. Correlation of observed K_d values for the cations with the hydration enthalpy difference between the acetate ion and the cationic species for (A) monovalent metal chlorides and (B) divalent metal chlorides.

and enzymes as well as their role in cell-signaling pathways and ligand−receptor binding events.[54−56] It should be noted that ion pairing is a saturation effect dominant in the low salt concentration regime. Once the binding sites became saturated, surface tension effects dominated instead. This caused some reordering of the LCST curves at high salt concentrations (Figures 1 and 2). Moreover, both surface tension and binding effects played a role at intermediate concentrations.

Since the ion pairing of cations with acetate follows the Hofmeister series, it is reasonable to ask if Hofmeister effects for this pairing interaction can be explained by the law of matching water affinity (LMWA).[35−37] As noted above, this idea predicts that ions of similar hydration energies will be thermodynamically favored to form ion-pairs rather than staying as separate entities in the aqueous solution. Moreover, questions have been raised as to whether such ion-pairing affinities could explain physiological phenomena, such as the generation of ion gradients across cell membranes.[20−22,50,52,57,58]

On the basis of the LMWA, carboxylate moieties attached to small molecules, peptides, polymers and proteins would be expected to have higher affinity toward similarly hydrated cations. This theory can be tested by correlating the abstracted K_d values of each cation from Table 1 with the hydration enthalpy differences between acetate and each cation. The enthalpy of hydration for acetate is −425.0 KJ/mol[46] and the values for the individual cations are given in Table 2. A plot of the difference between acetate's hydration enthalpy with respect to each monovalent cation versus the apparent K_d value of the binding pair is provided in Figure 8A. On the basis of the LMWA, it would be expected that the Na^+-acetate binding pair would be the tightest. More strongly and more weakly hydrated monovalent cations should pair with acetate to a lesser extent. As can be seen, the expected correlation is to some extent observed, but Li^+ and NH_4^+ are exceptions. Indeed, both of these metal ions bind more tightly than would be predicted by the model.

There are several reasons one may expect NH_4^+ to deviate from standard LMWA behavior. Specifically, this ion can interact with acetate via directional hydrogen bonding in addition to overall electrostatic affinity.[59] Moreover, it is possible to form multiple hydrogen bonds between one NH_4^+ and acetate either in an intermolecular or intramolecular fashion. By contrast, the tetramethyl ammonium cation, which has no hydrogen bonding capability, comes closer to the expected LMWA trend. Next, Li^+ ions also bind more tightly than expected. This ion's position in the Hofmeister series is known to shift depending upon the surrounding chemical context.[60] Li^+ is the smallest monovalent cation and binds it waters more tightly than other monovalent metal cations.[61,62] MD simulations have suggested that Na^+ would bind to acetate mostly via contact ion pairing, while Li^+ would be more prone to form solvent shared ion pairs.[21] Although the ratio of contact and solvent shared ion pairing may ultimately explain the Li^+ ion's somewhat anomalous behavior, further spectroscopic studies will be required to probe this subject in more detail.

The methodology described above for monovalent cations and the LMWA was also extended to divalent cations (Figure 8B). As can be seen, the correlation between the LMWA and the K_d values for acetate-divalent cation pairing was quite poor. In fact, there appears to be no trend in ion pairing with respect to the heats of hydration for the various divalent cations. This means that factors other than those associated with relative hydration enthalpy must dominate the process. One possibility involves the specific electronic structures of the various metal cations. In any case, it appears that the charge on an ion, its hydrogen bonding capability, as well as its specific electronic structure may play a role in determining cation−anion pairing in aqueous solution. These factors may all need to be taken into account in addition to considerations of the ions' relative sizes, which is at the heart of the LMWA model.[56,63−65]

Finally, it should also be noted that ELP DV_2F-64 contains 16 phenylalanine residues. These aromatic side chains could potentially play a role in cation partitioning to the protein surface via cation-π interactions.[66,67] However, such interactions are known to be substantially weaker than ion pairing interactions and become even more attenuated when the cations are freely mobile and solvated.[68−70] In the VSFS experiments performed at the air−water interface, the hydrophobic phenylalanine moieties should largely be pointing upward into the air and as such are not available for binding with the cations. The lack of ion specificity under protonated conditions in Figures 6 and 7 is a good indication that the ion specificity measured by VSFS comes exclusively from the deprotonated acetates. Moreover, the LCST measurements done at low pH also confirmed this idea as those curves are purely linear (Supporting Information Figure S2). Indeed, under acidic conditions the LCST decrease was very small and mostly not cation specific. Therefore, any cation−π interactions are assumed to be very weak, if they are present at all.

dx.doi.org/10.1021/jp212243c | J. Phys. Chem. B 2012, 116, 7389−7397

■ ASSOCIATED CONTENT

Supporting Information

Additional LCST measurements as a function of pH and VSFS measurements in D_2O. This material is available free of charge via the Internet at http://pubs.acs.org.

■ AUTHOR INFORMATION

Corresponding Author

*E-mail: Cremer@mail.chem.tamu.edu.

Notes

The authors declare no competing financial interest.

■ ACKNOWLEDGMENTS

We thank National Science Foundation (CHE-423121) and the Robert A. Welch Foundation (Grant A-1421) for funding. We also thank Prof. Ashutosh Chilkoti (Department of Biomedical Engineering, Duke University) for providing the DNA plasmids for ELP DV_2F-64. We would also like to thank Dr. Tinglu Yang for useful discussions.

■ REFERENCES

(1) Hofmeister, F. *Arch. Exp. Pathol. Pharmakol.* **1888**, *24*, 247−260.
(2) Kunz, W.; Henle, J.; Ninham, B. W. *Curr. Opin. Colloid Interface Sci.* **2004**, *9*, 19−37.
(3) Collins, K. D.; Washabaugh, M. W. *Q. Rev. Biophys.* **1985**, *18*, 323−422.
(4) Cacace, M. G.; Landau, E. M.; Ramsden, J. J. *Q. Rev. Biophys.* **1997**, *30*, 241−277.
(5) Baldwin, R. L. *Biophys. J.* **1996**, *71*, 2056−2063.
(6) Kunz, W.; Nostro, P. L.; Ninham, B. W. *Curr. Opin. Colloid Interface Sci.* **2004**, *9*, 1−18.
(7) Zhang, Y.; Cremer, P. S. *Curr. Opin. Chem. Biol.* **2006**, *10*, 658−663.
(8) Zangi, R.; Hagen, M.; Berne, B. J. *J. Am. Chem. Soc.* **2007**, *129*, 4678−4686.
(9) Ebel, C.; Pierre, F.; Kernel, B.; Zaccai, G. *Biochemistry* **1999**, *38*, 9039−9047.
(10) Wolff, J.; Sackett, D. L.; Knipling, L. *Proc. Sci.* **1996**, *5*, 2020−2028.
(11) Renoncourt, A.; Vlachy, N.; Bauduin, P.; Drechsler, M.; Touraud, D.; Verbavatz, J.-M.; Dubois, M.; Kunz, W.; Ninham, B. W. *Langmuir* **2007**, *23*, 2376−2381.
(12) Jäger, C. M.; Hirsch, A.; Schade, B.; Bötcher, C.; Clark, T. *Chem.—Eur. J.* **2009**, *15*, 8586−8592.
(13) Omta, A. W.; Kropman, M. F.; Wountersen, S.; Bakker, H. J. *Science* **2003**, *301*, 347−349.
(14) Zhang, Y.; Furyk, S.; Bergbreiter, D. E.; Cremer, P. S. *J. Am. Chem. Soc.* **2005**, *127*, 14505−14510.
(15) Cho, Y.; Zhang, Y.; Christensen, T.; Sagle, L. B.; Chilkoti, A.; Cremer, P. S. *J. Phys. Chem. B.* **2008**, *112*, 13765−13771.
(16) Lund, M.; Vrbka, L.; Jungwirth, P. *J. Am. Chem. Soc.* **2008**, *130*, 11582−11583.
(17) Robinson, D. R.; Jencks, W. P. *J. Am. Chem. Soc.* **1965**, *87*, 2470−2479.
(18) Patra, L.; Vidyasagar, A.; Toomey, R. *Soft Matter* **2011**, *7*, 6061−6067.
(19) Rembert, K. B.; Paterova, J.; Heyda, J.; Hilty, C.; Jungwirth, P.; Cremer, P. S. *J. Am. Chem. Soc.* **2012**, *134*, 10039−10046.
(20) Vrbka, L.; Vondrášek, J.; Jagoda-Cwiklik, B.; Vácha, R.; Jungwirth, P. *Proc. Natl. Acad. Sci. U. S. A.* **2006**, *103*, 15440−15444.
(21) Hess, B.; van der Vegt, N. F. A. *Proc. Natl. Acad. Sci. U. S. A.* **2009**, *106*, 13296−13300.
(22) Jagoda-Cwiklik, B.; Vácha, R.; Lund, M.; Srebro, M.; Jungwirth, P. *J. Phys. Chem. B* **2007**, *111*, 14077−14079.
(23) Ikegami, A.; Imai, N. *J. Polym. Sci.* **1962**, *56*, 133−152.
(24) Gregor, H. P.; Hamilton, M. J.; Oza, R. J.; Bernstein, F. *J .Phys. Chem.* **1956**, *60*, 263−267.
(25) Newman, J. K.; McCormick, C. L. *Macromolecules* **1994**, *27*, 5114−5122.
(26) Strauss, U. P.; Leung, Y. P. *J. Am. Chem. Soc.* **1965**, *87*, 1476−1480.
(27) Nagata, I.; Okamoto, Y. *Macromolecules* **1983**, *16*, 749−753.
(28) Sabbagh, I.; Delsanti, M. *Eur. Phys. J. E* **2000**, *1*, 75−86.
(29) Shen, Y. R. *The Principle of Nonlinear Optics*; John Wiley & Sons: New York, 1984.
(30) Richmond, G. L. *Chem. Rev.* **2002**, *102*, 2693−2724.
(31) Chen, X.; Yang, T.; Kataoka, S.; Cremer, P. S. *J. Am. Chem. Soc.* **2007**, *129*, 12272−12279.
(32) Chen, X.; Flores, S. C; Lim, S. M.; Zhang, Y.; Yang, T.; Kherb, J.; Cremer, P. S. *Langmuir* **2010**, *26*, 16447−16454.
(33) Meyer, D. E.; Chilkoti, A. *Nat. Biotechnol.* **1999**, *17*, 1112−1115.
(34) Cho, Y.; Sagle, L. B.; Iimura, S.; Zhang, Y.; Kherb, J.; Chilkoti, A.; Scholtz, J. M.; Cremer, P. S. *J. Am. Chem. Soc.* **2009**, *131*, 15188−15193.
(35) Collins, K. D. *Proc. Natl. Acad. Sci. U. S. A.* **1995**, *92*, 5553−5557.
(36) Collins, K. D. *Methods* **2004**, *34*, 300−311.
(37) Collins, K. D.; Neilson, G. W.; Enderby, J. E. *Biohys. Chem.* **2007**, *128*, 95−104.
(38) Shkol'nikov, E. V. *Russ. J. Appl. Chem.* **2004**, *77*, 1255−1258.
(39) Gurau, M. C.; Kim, G.; Lim, S. M.; Albertorio, F.; Fleisher, H. C.; Cremer, P. S. *Chem. Phys. Chem.* **2003**, *4*, 1231−1233.
(40) Meyer, D. E.; Chilkoti, A. *Biomacromolecules* **2002**, *3*, 357−367.
(41) Zhang, Y.; Cremer, P. S. *Proc. Natl. Acad. Sci. U. S. A.* **2009**, *106*, 15249−15253.
(42) Boström, M.; Parsons, D. F.; Salis, A.; Ninham, B. W.; Monduzzi, M. *Langmuir* **2011**, *27*, 9504−9511.
(43) Salis, A.; Cugia, F.; Parsons, D. F.; Ninham, B. W.; Monduzzi, M. *Phys. Chem. Chem. Phys.* **2012**, *14*, 4343−4346.
(44) Weissenborn, P. K.; Pugh, R. J. *J. Colloid Interface Sci.* **1996**, *184*, 550−563.
(45) Pegram, L. M.; Record, M. T., Jr. *J. Phys. Chem. B* **2007**, *111*, 5411−5417.
(46) Marcus, Y. *Ion Properties*; Marcel Dekker: 1997.
(47) Manning, G. S. *Q. Rev. Biophys.* **1978**, *11*, 179−246.
(48) Begala, J. A.; Strauss, U. P. *J. Phys. Chem.* **1972**, *76*, 254−260.
(49) Bulo, R. E.; Donadio, D.; Laio, A.; Molnar, F.; Rieger, J.; Parrinello. *Macromolecules* **2007**, *40*, 3437−3442.
(50) Mattai, J.; Kwak, J. C. T. *Macromolecules* **1986**, *19*, 1663−1667.
(51) Gustafson, R. L.; Lirio, J. A. *J. Phys. Chem.* **1968**, *72*, 1502−1505.
(52) Tang, C. Y.; Huang, Z.; Allen, H. C. *J. Phys. Chem. B* **2011**, *115*, 34−40.
(53) Dudev, T.; Lim, C. *Chem. Rev.* **2003**, *103*, 773−787.
(54) Hamm, L. M.; Wallace, A. F.; Dove, P. M. *J. Phys. Chem. B* **2010**, *114*, 10488−10495.
(55) Stryer, L. *Biochemistry*, 4th ed.; W. H. Freeman and Co.: New York, 1995.
(56) Babu, C. S.; Dudev, T.; Casareno, R.; Cowan, J. A.; Lim, C. *J. Am. Chem. Soc.* **2003**, *125*, 9318−9328.
(57) Vácha, R.; Jurkiewicz, P.; Petrov, M.; Berkowitz, M. L.; Böckmann, R. A.; Barucha-Kraszewska, J.; Hof, M.; Jungwirth, P. *J. Phys. Chem. B* **2010**, *114*, 9504−9509.
(58) Vlachy, N.; Jagoda-Cwiklik, B..; Vacha, R.; Touraud, D.; Jungwirth, P.; Kunz, W. *Adv. Colloid Interface Sci.* **2009**, *146*, 42−47.
(59) Sada, K.; Tani, T.; Shinkai, S. *Synlett* **2006**, *15*, 2364−2374.
(60) Horinek, D.; Herz, A.; Vrbka, L.; Sedlmeier, F.; Mamatkulov, S. I.; Netz, R. R. *Chem. Phy. Lett.* **2009**, *479*, 173−183.
(61) Loeffler, H. H.; Rode, B. M. *J. Chem. Phys.* **2002**, *117*, 110−117.
(62) Varma, S.; Rempe, S. B. *Biophys. Chem.* **2006**, *124*, 192−199.
(63) Dudev, T.; Carmay, L. *Acc. Chem. Res.* **2007**, *40*, 85−93.
(64) Marcus, Y.; Hefter, G. *Chem. Rev.* **2006**, *106*, 4585−4621.
(65) Ryde, U. *Biophys. J.* **1999**, *77*, 2777−2787.
(66) Dougherty, D. A. *Science* **1996**, *271*, 163−168.

(67) Gallivan, J. P.; Dougherty, D. A. *Proc. Natl. Acad. Sci. U. S. A.* **1999**, *96*, 9459−9464.
(68) Meyer, E. A.; Castellano, R. K.; Diederich, F. *Ang. Chem. Int. Ed.* **2003**, *42*, 1210−1250.
(69) Reddy, A. S.; Zipse, H.; Sastry, G. N. *J. Phys. Chem. B* **2007**, *111*, 11546−11553.
(70) Rao, J. S.; Zipse, H.; Sastry, G. N. J *Phys. Chem. B* **2009**, *113*, 7225−7236.